CORA Cork Open Research Archive
Cartlann Taighde Oscailte Chorcaí

Title	Competitive carrier interactions influencing the emission dynamics of GaAsSb-capped InAs quantum dots
Authors	Pavarelli, Nicola;Ochalski, Tomasz J.;Liu, H. Y.;Gradkowski, Kamil;Schmidt, Michael;Williams, David P.;Mowbray, D. J.;Huyet, Guillaume
Publication date	2012
Original Citation	Pavarelli, N., Ochalski, T. J., Liu, H. Y., Gradkowski, K., Schmidt, M., Williams, D. P., Mowbray, D. J. and Huyet, G. (2012) 'Competitive carrier interactions influencing the emission dynamics of GaAsSb-capped InAs quantum dots', Applied Physics Letters, 101(23), pp. 231109. doi: 10.1063/1.4769431
Type of publication	Article (peer-reviewed)
Link to publisher's version	http://aip.scitation.org/doi/abs/10.1063/1.4769431 - 10.1063/1.4769431
Rights	© 2012 American Institute of Physics.This article may be downloaded for personal use only. Any other use requires prior permission of the author and AIP Publishing. The following article appeared in Pavarelli, N., Ochalski, T. J., Liu, H. Y., Gradkowski, K., Schmidt, M., Williams, D. P., Mowbray, D. J. and Huyet, G. (2012) 'Competitive carrier interactions influencing the emission dynamics of GaAsSb-capped InAs quantum dots', Applied Physics Letters, 101(23), pp. 231109 and may be found at http://aip.scitation.org/doi/abs/10.1063/1.4769431
Download date	2024-04-20 10:10:50
Item downloaded from	https://hdl.handle.net/10468/4293

University College Cork, Ireland
Coláiste na hOllscoile Corcaigh

Competitive carrier interactions influencing the emission dynamics of GaAsSb-capped InAs quantum dots

N. Pavarelli, T. J. Ochalski' , H. Y. Liu, K. Gradkowski, M. Schmidt, D. P. Williams, D. J. Mowbray, and G. Huyet

Citation: Appl. Phys. Lett. **101**, 231109 (2012); doi: 10.1063/1.4769431
View online: http://dx.doi.org/10.1063/1.4769431
View Table of Contents: http://aip.scitation.org/toc/apl/101/23
Published by the American Institute of Physics

Competitive carrier interactions influencing the emission dynamics of GaAsSb-capped InAs quantum dots

N. Pavarelli,[1,2] T. J. Ochalski,[1,2,a)] H. Y. Liu,[3] K. Gradkowski,[1,2] M. Schmidt,[1] D. P. Williams,[1,2] D. J. Mowbray,[4] and G. Huyet[1,2]
[1]*Tyndall National Institute, University College Cork, Cork, Ireland*
[2]*Centre for Advanced Photonics and Process Analysis, Cork Institute of Technology, Cork, Ireland*
[3]*Department of Electronic and Electrical Engineering, University College London, Torrington Place, London WC1E 7JE, United Kingdom*
[4]*Department of Physics and Astronomy, University of Sheffield, Sheffield S3 7RH, United Kingdom*

(Received 10 September 2012; accepted 15 November 2012; published online 6 December 2012)

The optical properties of InAs/GaAs quantum dots capped with a GaAsSb quantum well are investigated by means of power-dependent and time-resolved photoluminescence. The structure exhibits the coexistence of a type-I ground state and few type-II excited states, the latter characterized by a simultaneous carrier density shift of the peak position and wavelength-dependent carrier lifetimes. Complex emission dynamics are observed under a high-power excitation regime, with the different states undergoing shifts during specific phases of the measurement. These features are satisfactorily explained in terms of band structure and energy level modifications induced by two competitive carrier interactions inside the structure. © *2012 American Institute of Physics*. [http://dx.doi.org/10.1063/1.4769431]

Semiconductor quantum dots (QDs)[1] have been extensively investigated in the past decade, and because of their unique physical properties arising from the quantum confinement of carriers in all three spatial dimensions, they are now widely employed for the realization of a number of optoelectronics devices. In particular, high-quality type-I In(Ga)As/GaAs QDs, where both electrons and holes are confined within the dot, have been used as the active material for near infrared lasers in the 1.3 μm telecommunication window.[2,3] Recently, In(Ga)As/GaAs QDs capped with InGaAs or GaAsSb quantum well (QW) have created interest. The larger QW lattice constant compared to GaAs reduces the strain induced in the QDs during the capping process, preserving the shape, and reducing the decomposition of the dots.[4–6] Moreover, contrary to other strain-relieving layers, GaAsSb QW with 14% Sb keeps the confining potential of both electrons and holes essentially identical to that of InAs QDs in GaAs matrix. This limits the carrier thermal escape from the QDs and consequently leads to optimized emission intensity and spectral width,[7,8] although the spatial localization of the holes is reduced. A further increment of Sb concentration in the QW results in a type-I to type-II band alignment transition.[9,10] The spatial separation of carriers created by the type-II structure (the electrons are in the QDs while the holes are in the QW) significantly reduces the carrier wavefunctions overlap and, consequently, the emission probability.

In this work, we report the optical characterization of a single layer of high-quality self-assembled MBE-grown InAs/GaAs QDs capped by a 6 nm thick $GaAs_{0.86}Sb_{0.14}$ QW. Further details of the growth conditions can be found in Refs. 7 and 11. The Sb concentration in the QW was chosen for the investigation of the optical emission properties at the transition point between type-I and type-II band alignment, where the structure is expected to exhibit not only the most enhanced luminescence characteristics but also unique physical phenomena. The study was performed at low temperature (10 K) by means of power-dependent photoluminescence (PL) and time-resolved PL (TRPL) measurements. PL experiments were performed using a standard setup equipped with a 660 nm CW semiconductor laser, a 0.5 m monochromator, an InGaAs APD detector, and a lock-in amplifier. TRPL experiments were performed employing a 780 nm, 75.6 MHz, 300 fs mode-locked Ti:sapphire laser as the excitation source, and a streak camera as the detection system. The temporal resolution of the experiment was ~20 ps. The band structure of the QDs was calculated by means of an 8-band strain-dependent $\mathbf{k}\cdot\mathbf{p}$ model (see Ref. 12, and references therein for details). The QDs were simulated as truncated pyramids (16 nm × 16 nm in base size and 4 nm in height) containing 90% In and capped with a GaAsSb QW of appropriate thickness (6 nm) and composition (14% Sb). The material parameters for the calculations were taken from Ref. 13.

Figure 1 shows the calculated band structure. In the conduction band the QD forms a deep confining potential (~0.41 eV) with a small number of confined electron levels. The valence band is more complicated because the energy difference between QD and QW valence band edges is small, less than 30 meV. The two lowest hole levels are shown in the band diagram. The first, double-degenerate, hole level (H_{QD}) lies in the QD ~40 meV below the QD band edge, while the second hole level (H_{QW}) is in the QW just ~2 meV below H_{QD}. H_{QD} and H_{QW} wave-functions, depicted in the two insets of Fig. 1, were also calculated. H_{QD} is mainly confined inside the QD, although the tails of its wave-function penetrate the surrounding QW. For H_{QW} the situation is reversed, its wave-function is mostly confined in the QW and it slightly penetrates the QD at the sides of the pyramid. The optical matrix elements of all possible radiative recombination channels involving the first two hole levels and the

a)Author to whom correspondence should be addressed. Electronic mail: tomasz.ochalski@tyndall.ie.

 © 2012 American Institute of Physics

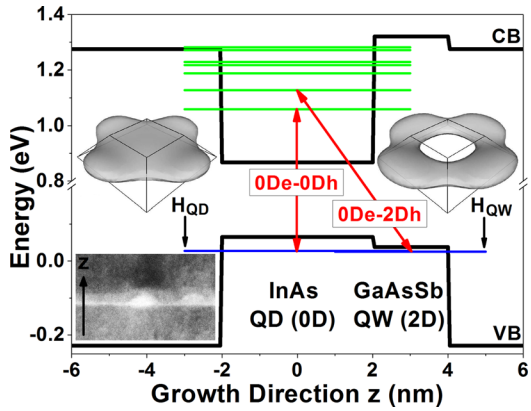

FIG. 1. Band structure calculated along the growth direction z and centred on the QD. The red arrows represent the most probable radiative recombination channels. The iso-surfaces at 50% amplitude are used to represent the calculated wave-functions for the first two hole levels (H_{QD} and H_{QW}, respectively). The outline of the dot is provided for visual reference. A cross-section high-angle annular dark field scanning transmission electron microscopy (HAADF STEM) image is also depicted in the inset.

first two electron levels (E_0 and E_1, both in the QD) are reported in Table I. E_0-H_{QD} and E_1-H_{QW} show the highest wave-function overlaps, therefore, the most probable optical transitions are a type-I ground state (GS) occurring between electrons and holes both confined in the dot (0De-0Dh red arrow in Fig. 1) and a type-II excited state (ES) occurring between electrons in the dot and holes in the well (0De-2Dh red arrow in Fig. 1).

However, the analysis above refers to an ideal case defined by specific QD and QW, and therefore, it does not take into account the inhomogeneous broadening of the real structure. Because of the small size of the valence band offset, the distribution in dot size and dot/well composition may result in a change or even a reversal of the valence band offset. In the case of a slight change in valence band offset without a reversal, the H_{QD} and H_{QW} hole wave-function shapes remain largely unaltered, leading to similar optical matrix elements and transitions as those calculated. In the case of a reversal of the band offset, there will no longer be a dot-like wave-function, and the GS hole wave-function will look similar to H_{QW}. Consequently, it will have similar optical matrix elements, and there will be no significant radiative recombination between it and E_0, i.e., these QDs will not contribute to the observed GS emission. Therefore, the effect of the inhomogeneous broadening will not dramatically modify the calculated radiative transition channels.

Figure 2 shows the combination of power-dependent PL and TRPL results. The PL spectrum (black continuous line) measured at 500 W/cm^2 exhibits three separate features, corresponding to the first three radiative recombination channels, i.e., GS and two ESs. The peak position for the three states is calculated by fitting the emission intensity versus the wavelength by a tri-Gaussian function. The GS emission occurs at 1203 nm (1.031 eV), while the two ESs are centred at 1124 nm (1.103 eV) and 1062 nm (1.168 eV), respectively. The behaviour of these features as a function of the power density, presented in the inset B of Fig. 2, is different. The type-I GS peak position remains constant, while the type-II ES peaks shift toward longer wavelengths (lower energies) with decreasing power density. The energy shift (ΔE) within the explored range of power densities (P) for the first ES (ES1) is 8 meV, while the second ES (ES2) is not detected for P below 100 W/cm^2 and therefore is not shown here. This red-shift can be explained in terms of electron and hole energy level modifications due to the Coulomb interactions between the spatially separated carriers.[14–16] The QW wave-functions are relatively weakly confined compared to the QD wave-functions, so that the magnitude of the Coulomb potential due to the electrons is much stronger than that due to the holes. Hence the change in energy level of the electrons in the dot is dominated by the repulsion between the electrons, pushing their energy levels up and out of the dot. For the holes in the well, the attraction to the electrons in the dot greatly increases the confinement of their wave-functions and decreases their energy with respect to the QW band edge. The overall result is an increase in the electron-hole recombination energy, the magnitude of which is proportional to the number of photo-generated carriers inside the structure, explaining the net increase of the ES emission energies with increasing excitation power.

The character of the observed peaks is also analyzed by using TRPL measurements under a similar power density regime. The decay profiles for the three distinct peaks are shown in the inset A of Fig. 2, while the decay times (colored open symbols) presented in Fig. 2 are calculated as a function of the wavelength by fitting the corresponding decay profiles with a single exponential function. For the GS, the decay times do not significantly change with wavelength, confirming the type-I character of this emission. The average GS carrier lifetime is 1.26 ns, and has a standard

TABLE I. Calculated optical matrix elements for all possible radiative recombination channels involving the first two electron (E_0 and E_1) and the first two hole (H_{QD} and H_{QW}) levels.

Levels	H_{QD}	H_{QW}
E_0	33.75	0.001
E_1	0.006	24.02

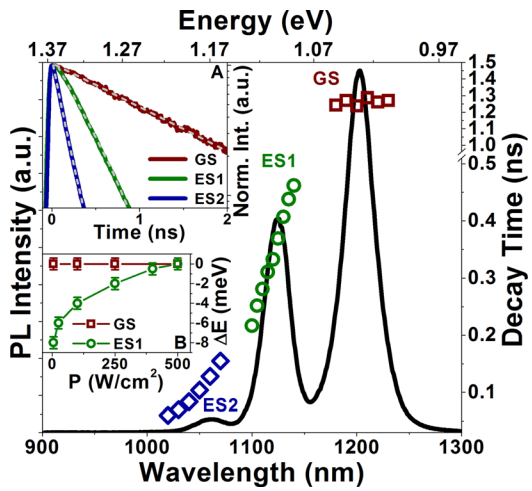

FIG. 2. Combination of power-dependent PL and TRPL experimental results measured at T = 10 K. The peak position versus the power density for GS and ES1 is depicted in the inset B. The decay times extracted for selected wavelengths are represented by colored opened symbols. The decay profiles corresponding to each separate emission and their single exponential fits (grey dashed lines) are depicted in the inset A.

deviation which is comparable with the temporal resolution of the experiment. This value is consistent with the decay times measured at low temperature for conventional InAs/GaAs QDs.[17] A different behaviour is observed for the two ESs, where the carrier lifetimes measured at the short-wavelength side of each peak are much shorter than those measured at the long-wavelength side. Such strong wavelength-dependent emission dynamics represents, together with the red-shift of the peak position with decreasing excitation powers, another characteristic of type-II band aligned heterostructures.[18,19] After the photo-generation of e-h pairs inside the structure, the spectrum is blue-shifted and, due to the strong attraction between the electrons in the dot and the holes in the well, the overlap between the carrier wave-functions is at its maximum. The associated emission dynamics (the decay time is inversely proportional to the square of this wave-function overlap) is therefore fast. Following radiative recombination, the carrier density decreases, the spectrum undergoes a red-shift, the wave-function overlap is reduced, and consequently the emission dynamics become slower. In this particular case, the decay times vary from 220 ps to 460 ps for ES1 and from 60 ps to 150 ps for ES2. The high-energy electron levels in the QD efficiently thermalize to the GS. The ESs decay times are therefore much faster, regardless their type-II character, than that of the type-I GS.

Figure 3 shows the emission dynamics for the high-power density regime ($P = \sim 3\,MW/cm^2$) by means of a streak image. The position of the maximum of the intensity for the three states is shown by the black lines. Immediately after the laser pulse ($t = 0$), when the carrier density in the structure is the highest, the GS emission peak is red-shifted by ~ 11 meV with respect to its few-carrier position. This shift was not observed in Fig. 2 because of the much lower power density employed in the PL experiment. The relaxation of the emission toward its final wavelength of 1203 nm occurs during the first ~ 1.1 ns, after that time the peak position remains constant until the end of the decay ($t = 4$ ns). Contrary to the GS, the temporal evolution of the ES1 emission peak is not monotonic. It experiences an initial blue-shift for the first ~ 0.25 ns, then it reverses direction and a red-shift is observed until the emission is no longer visible after ~ 1.5 ns. ES2 behaves similarly to ES1, even though the initial blue-shift is not that clear from the streak image. Additional information on the emission dynamics can be obtained by extracting the decay profiles for the three distinct peaks seen in the streak image. Each decay profile, presented in the inset of Fig. 3, shows common features. After the initial fast capture of the e-h pairs generated by the laser pulse (represented by the steep intensity increase occurring within the temporal resolution of the experiment), the decay profiles exhibit a smooth rise and, only after the maximum of the intensity is reached, an exponential decay. The duration of this rise is ~ 0.7 ns for the GS and ~ 0.15 ns for the ES1.

The various phases exhibited by the emission dynamics can be satisfactorily explained by considering the modifications to the band structure induced by the potentials arising from the interactions between the carriers generated inside the structure under different power density regimes. The two band structures in Figs. 4(b) and 4(c) schematically show these modifications, together with the related change in energy levels of electrons and holes, for low-power and high-power density, respectively. The unperturbed band structure, previously depicted in Fig. 1, is presented again in Fig. 4(a) for comparison. When the material is excited under low-power density, the different densities of states between the QD and the QW mean that, following GS occupation, the holes begin to fill the well states, while the electrons continue to fill the ESs within the dot. Since the repulsion between the confined electrons represents the major contribution to the carrier interactions, the Coulomb potential is centred on the dot. As a result both electron and hole, QD states experience similar shifts toward higher energies, resulting in little change of the overall GS recombination energy. However, the hole states in the QW experience a significant increase in their confinement energy which, together with a smaller band-edge shift, leads to an increase in the separation between the QW hole and QD electron levels. This causes the increase of the ESs emission energy [represented by the orange arrow in Fig. 4(b)], while the GS emission energy [red arrow in Fig. 4(b)] remains approximately constant.

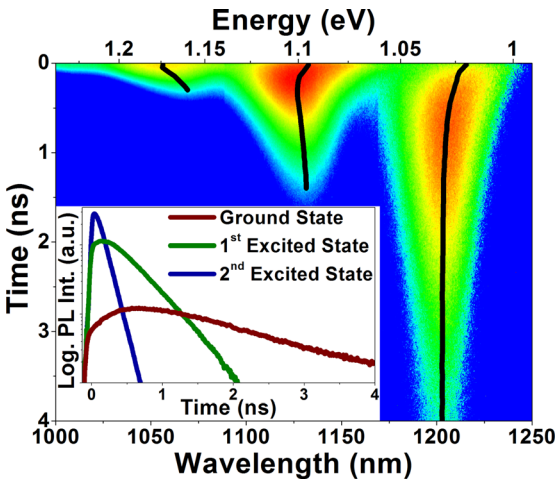

FIG. 3. Streak image [representing the logarithm of the emission intensity in color scale as a function of wavelength (energy) and time] measured at $T = 10$ K under high-power density regime. The black lines show the temporal evolution of the peak position for the three observed features. The decay profiles corresponding to each separate emission are depicted in the inset.

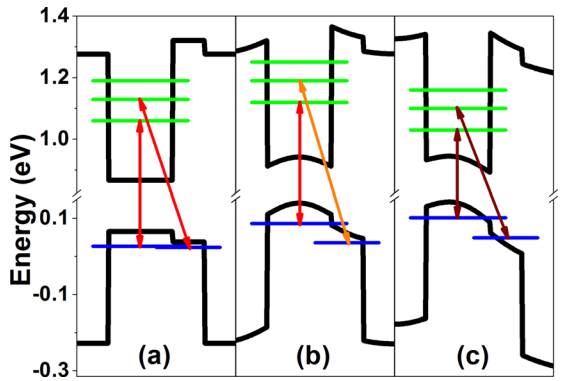

FIG. 4. Schematic profile of (a) unperturbed band structure, (b) perturbed band structure under low-power density, and (c) perturbed band structure under high-power density. Orange arrows indicate an increase, while brown arrows indicate a decrease of optical transition energy in comparison with the unperturbed case.

Under the high-power density regime, a much higher number of e-h pairs are created inside the structure than the number of available electrons states within the dots. Therefore, after the dots are completely full, since the QW acts as a potential barrier for the carriers in conduction band, excess electrons begin to fill the bulk states in the wetting layer underneath the QDs, while the majority of the holes are still captured by the GaAsSb well. Hence, two charged carrier layers with opposite sign are formed above and below the dots resulting in an internal electric field across the structure. This field, acting similarly to the quantum-confined Stark effect, causes a reduction of the recombination energy for all the states,[20] as depicted by the brown arrows in Fig. 4(c). This is the physical origin of the shift observed in the streak image immediately after the excitation pulse ($t = 0$). From this time onwards, radiative recombination depletes the carrier population in the structure, the electric field decreases and the emissions shift toward shorter wavelengths. After this initial blue-shift, once the strength of the electric field becomes comparable with the magnitude of the Coulomb interactions, the emission dynamics become governed by the superimposition of the two competitive effects. With elapsing time, due to the progressive reduction of the external electric field, the Coulomb interactions become dominant, and both ESs red-shift according to their type-II behaviour. On the other hand, the GS emission energy, which is not affected by the Coulomb interactions, undergoes only the initial blue-shift during the early stage of the decay.

The complicated shape of the decay profiles in the inset of Fig. 3 cannot be explained simply in terms of QD saturation, where the relaxation of carriers from higher energy states maintains a constant GS population.[21] This cannot replicate the slow intensity rise after the fast carrier capture and the fact that the intensity maximum is reached after a significant time delay. Instead, these features are a consequence of the suppression of the spontaneous emission of the low-energy states due to the occupation of the high-energy ones. The large number of carriers in the high-energy levels in the valence band does not participate in the radiative processes but exert an inhibition on the recombination rate for the low-energy transitions.[20] This also explains why the time duration of the rise is different between the GS and the ES1, with the former clearly showing the most pronounced effect since it is the lowest energy state in the structure. Moreover, the exponential decay for a general state N starts only when the population of the state $N + 1$ (and all the states energetically above) is—because of radiative recombination—significantly reduced. This occurs after $\sim$1.85 ns for the GS and after $\sim$0.55 ns for the ES1.

In conclusion, we have studied the optical emission properties of a single layer of InAs QDs capped by a $GaAs_{0.86}Sb_{0.14}$ QW. This specific content of Sb was chosen to investigate the structure at the boundary between type-I and type-II, since the QW and QD valence band edges lie approximately at the same level. Under low-power density regime, power-dependent PL and TRPL experimental results showed that a type-I GS and type-II ESs coexist in the same structure. The type-II ES transitions are characterized by both red-shift of the peak position with decreasing excitation power and wavelength-dependent emission dynamics, while for the type-I GS transition the peak position and the decay time are invariant. Under a high-power density regime, the character of the optical transitions is conserved. However, the structure exhibited complex dynamics, which are explained in terms of band structure and energy level modifications induced by two distinct and competitive potentials created by the carrier interactions. In such structures, due to the type-II character of the ESs, their lasing threshold is expected to be greater than that of conventional type-I QDs. Therefore, the employment of GaAsSb capping layer in InAs/GaAs QD-based lasers should block the lasing from high-energy states, resulting in a stable GS lasing even at high currents.

This work was supported by Science Foundation Ireland (Grant Nos. 07/IN.1/I929 and 09/SIRG/I1621), Enterprise Ireland (Grant No. RE/2007/006), and the INSPIRE programme under the HEA PRTLI Cycle 4, National Development Plan 2007-2013.

[1]D. Bimberg, M. Grundmann, and N. N. Ledentsov, *Quantum Dot Heterostructures* (Wiley, New York, 1999).
[2]G. Park, O. B. Shchekin, S. Csutak, D. L. Huffaker, and D. G. Deppe, Appl. Phys. Lett. **75**, 3267 (1999).
[3]A. E. Zhukov, A. R. Kovsh, N. A. Maleev, S. S. Mikhrin, V. M. Ustinov, A. F. Tsatsul'nikov, M. V. Maximov, B. V. Volovik, D. A. Bedarev, Yu. M. Shernyakov, P. S. Kop'ev, Zh. I. Alferov, N. N. Ledentsov, and D. Bimberg, Appl. Phys. Lett **75**, 1926 (1999).
[4]J. M. Ulloa, I. W. D. Drouzas, P. M. Koenraad, D. J. Mowbray, M. J. Steer, H. Y. Liu, and M. Hopkinson, Appl. Phys. Lett. **90**, 213105 (2007).
[5]J. M. Ulloa, C. Çelebi, P. M. Koenraad, A. Simon, E. Gapihan, A. Letoublon, N. Bertru, I. Drouzas, D. J. Mowbray, M. J. Steer, and M. Hopkinson, J. Appl. Phys. **101**, 081707 (2007).
[6]J. M. Ulloa, P. M. Koenraad, M. Bonnet-Eymard, A. Letoublon, and N. Bertru, J. Appl. Phys. **107**, 074309 (2010).
[7]H. Y. Liu, M. J. Steer, T. J. Badcock, D. J. Mowbray, M. S. Skolnick, P. Navaretti, K. M. Groom, M. Hopkinson, and R. A. Hogg, Appl. Phys. Lett. **86**, 143108 (2005).
[8]J. M. Ulloa, R. Gargallo-Caballero, M. Bozkurt, M. del Moral, A. Guzman, P. M. Koenraad, and A. Hierro, Phys. Rev. B **81**, 165305 (2010).
[9]M. Peter, K. Winkler, M. Maier, N. Herres, J. Wagner, D. Fekete, K. H. Bachem, and D. Richards, Appl. Phys. Lett. **67**, 2639 (1995).
[10]P. Klenovsky, V. Krapek, D. Munzar, and J. Humlicek, Appl. Phys. Lett. **97**, 203107 (2010).
[11]H. Y. Liu, M. J. Steer, T. J. Badcock, D. J. Mowbray, M. S. Skolnick, F. Suarez, J. S. Ng, M. Hopkinson, and J. P. R. David, J. Appl. Phys. **99**, 046104 (2006).
[12]K. Gradkowski, T. J. Ochalski, N. Pavarelli, H. Y. Liu, J. Tatebayashi, D. P. Williams, D. J. Mowbray, G. Huyet, and D. L. Huffaker, Phys. Rev. B **85**, 035432 (2012).
[13]I. Vurgaftman, J. R. Meyer, and L. R. Ram-Mohan, J. Appl. Phys. **89**, 5815 (2001).
[14]C. Y. Jin, H. Y. Liu, S. Y. Zhang, Q. Jiang, S. L. Liew, M. Hopkinson, T. J. Badcock, E. Nabavi, and D. J. Mowbray, Appl. Phys. Lett. **91**, 021102 (2007).
[15]W.-H. Chang, Y.-A. Liao, W.-T. Hsu, M.-C. Lee, P.-C. Chiu, and J.-I. Chyi, Appl. Phys. Lett. **93**, 033107 (2008).
[16]M. Ahmad Kamarudin, M. Hayne, R. J. Young, Q. D. Zhuang, T. Ben, and S. I. Molina, Phys. Rev. B **83**, 115311 (2011).
[17]E. Harbord, P. Spencer, E. Clarke, and R. Murray, Phys. Rev. B **80**, 195312 (2009).
[18]Y. D. Jang, T. J. Badcock, D. J. Mowbray, M. S. Skolnick, J. Park, D. Lee, H. Y. Liu, M. J. Steer, and M. Hopkinson, Appl. Phys. Lett. **92**, 251905 (2008).
[19]K. Gradkowski, N. Pavarelli, T. J. Ochalski, D. P. Williams, J. Tatebayashi, G. Huyet, E. P. O'Reilly, and D. L. Huffaker, Appl. Phys. Lett. **95**, 061102 (2009).
[20]K. Gradkowski, T. J. Ochalski, N. Pavarelli, D. P. Williams, G. Huyet, B. Liang, and D. L. Huffaker, Appl. Phys. Lett. **97**, 091105 (2010).
[21]R. Heitz, M. Veit, A. Kalburge, Q. Xie, M. Grundmann, P. Chen, N. N. Ledentsov, A. Hoffmann, A. Madhukar, D. Bimberg, V. M. Ustinov, P. S. Kop'ev, and Zh. I. Alferov, Physica E **2**, 578 (1998).